INSTITUTE OF PHYSICS PUBLISHING EUROPEAN JOURNAL OF PHYSICS

Eur. J. Phys. **26** (2005) 1085–1091 doi:10.1088/0143-0807/26/6/016

The effects of linear and quadratic drag on falling spheres: an undergraduate laboratory

Julia P Owen and William S Ryu

Lewis-Sigler Institute for Integrative Genomics, Princeton University, Princeton, NJ 08544, USA

E-mail: wsryu@princeton.edu

Received 22 June 2005, in final form 25 July 2005
Published 21 September 2005
Online at stacks.iop.org/EJP/26/1085

Abstract

A desktop experiment to demonstrate the linear and quadratic velocity dependence of drag on an object falling in a resistive medium was developed for an undergraduate laboratory. The motion of ball bearings dropped into a cylinder filled with fluid is captured and measured using computer-based imaging. The terminal velocity of falling spheres is measured as a function of size at low and high Reynolds number, and the results are compared to predicted scaling laws for models containing a drag force that is linear or quadratic with velocity.

1. Introduction

A popular topic of study for students in introductory physics is the description of objects falling through a resistive medium. The drag on an object is generally dependent on its velocity, v, and there exist two regimes where this dependence is either linear or quadratic. The parameter that differentiates these two regimes is the Reynolds number, Re, which is the ratio of inertial to viscous forces,

$$Re = \frac{\rho l v}{\eta}, \tag{1}$$

where ρ is the fluid density, l is the characteristic cross-sectional length, v is the velocity and η is the dynamic fluid viscosity. At high Reynolds number ($Re > 10^3$), drag is approximately dependent on the square of the velocity. Most textbook examples of falling objects (e.g. apples, projectiles, sky divers, etc) are high Reynolds phenomena. Less familiar are objects moving at low Reynolds number ($Re \ll 1$) [1]. For small objects, moving slowly, through a viscous fluid, such as motile microorganisms or sedimenting sand, drag is linear with velocity. While drag is sometimes introduced at the introductory level [2], the treatment is often cursory and the distinction between linear and quadratic drag is not discussed. When the drag force

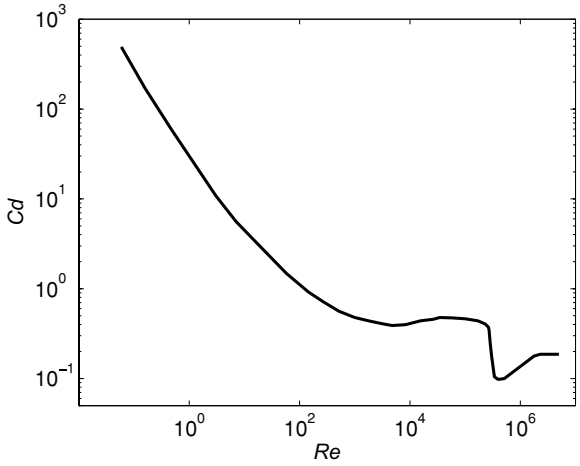

Figure 1. Drag coefficient (C_d) versus Reynolds number (Re) for flow past a sphere.

is linear or quadratic with velocity, analytic solutions to the equation of motions exist, and so with a little work a more comprehensive treatment can be given.

Unfortunately, demonstrating linear and quadratic drag in the laboratory is difficult due to the range of speeds typically needed to go from one regime to another. Laboratories incorporating drag have been published but they either focus on a single regime of drag or use outdated experimental techniques that can now be modernized [3, 4]. In our desktop experiment, the motions of small spheres falling in fluids at high and low Reynolds number are measured using computer video imaging. The students solve the equations of motion for falling spheres at high and low Reynolds number and determine how the terminal velocity should scale with the size of the spheres for the two models of drag. They then make measurements to verify their results.

2. Theory

The equation of motion for an object falling in a fluid is

$$m\frac{\mathrm{d}v}{\mathrm{d}t} = (m - m')g - f_d(v) = M'g - f_d(v), \tag{2}$$

where $f_d(v)$ is the velocity-dependent drag force and M' is the effective mass of the object corrected for buoyancy, $m'g$. For speeds below the onset of turbulence, the drag term can be written generally as

$$f(v) = \tfrac{1}{2}\rho C_d A v^2, \tag{3}$$

where ρ is the density of the fluid, C_d is the drag coefficient, A is the cross-sectional area and v is the velocity of the object. The drag coefficient, C_d, depends on the Reynolds number (figure 1) [5].

Numerous examples of curve fits to empirical data have been published [6]. Here we give one example that extends up to a Reynolds number of 2×10^5 [7],

$$C_d \approx \frac{24}{Re} + \frac{6}{1 + \sqrt{Re}} + 0.4. \tag{4}$$

2.1. Low Reynolds number

At low Reynolds number ($Re < 1$) the first term in equation (4) dominates. $Re \propto v$, so $C_d \propto 1/v$, making $f_d(v)$ linearly dependent with velocity. For a sphere of radius r and area $A = \pi r^2$, equation (3) becomes

$$f_d(v) = \frac{12\eta A v}{l} = 6\pi\eta r v. \tag{5}$$

This is the well-known equation for the Stokes drag force, which is valid at low Re. In this regime, inertial forces are negligible and viscous forces dominate. From (2), we see that the terminal velocity, v_{ter}, of a falling sphere is

$$v_{\text{ter}} = \frac{M'g}{6\pi\eta r}, \tag{6}$$

and that the general solution is

$$v(t) = v_{\text{ter}}(1 - \exp(-t/\tau)), \tag{7}$$

where $\tau = m/6\pi\eta r$. To determine how the terminal velocity scales with r we need to identify all factors that are dependent on the radius of the sphere. Since M' varies with the volume of the sphere, we get:

$$v_{\text{ter}} = \frac{M'(r)g}{6\pi\eta r} \propto \frac{r^3 g}{6\pi\eta r} \propto Cr^2, \tag{8}$$

where C contains terms independent of r. So the terminal velocity of a falling sphere at low Reynolds number is quadratic with the radius, $v_{\text{ter}} \propto r^2$.

2.2. High Reynolds number

At high Reynolds number ($10^3 < Re < 10^5$) we can see from figure 1 that C_d is approximately constant ($C_d \approx 0.4$). The equation of motion is

$$m\frac{\mathrm{d}v}{\mathrm{d}t} = mg - \frac{1}{2}\rho C_d A v^2, \tag{9}$$

where we assume $m \sim M'$. The terminal velocity, v_{ter}, is

$$v_{\text{ter}} = \left(\frac{2mg}{\rho C_d A}\right)^{1/2}, \tag{10}$$

and the general solution is

$$v(t) = v_{\text{ter}} \tanh\left(\frac{gt}{v_{\text{ter}}}\right). \tag{11}$$

All terms in equation (10) are constant with respect to sphere size (r), except for $m \propto r^3$ and $A \propto r^2$. So the terminal velocity of a falling sphere at high Reynolds number scales with the square root of the radius, $v_{\text{ter}} \propto r^{1/2}$.

3. The experiment

Ball bearings[1] made of aluminium and steel were dropped into graduated cylinders containing water or glycerol. A CMOS camera[2] with a 25 mm lens was placed approximately 1/2 m

[1] McMaster-Carr, Dayton, NJ.
[2] Model A601f, Basler Vision Technologies, Exton, PA.

from the cylinder and a piece of white cardboard was placed directly behind the cylinder to increase the contrast of the image. Video of falling spheres in fluid was captured using custom programs written in LabVIEW[3] on a PC. The images were analysed in ImageJ[4], and calculations and curve-fitting were done using MATLAB[5].

3.1. Low Reynolds number

To reach low Reynolds numbers we dropped aluminium spheres ($r = 0.08$–0.16 cm) in a 100 ml graduated cylinder filled with 98% glycerol[6] at room temperature. The glycerol viscosity at room temperature was measured to be 9.34 g cm^{-3} using a Cannon–Fenske routine viscometer and the density of the glycerol was taken to be 1.26 g cm^{-3}. With an exponential time constant of $\tau < 1$ ms (see equation (7)), the approach to terminal velocity was too fast to be measured, as expected.

The images of the gracefully falling spheres were captured at one or two frames per second. Images were imported into ImageJ, and the x- and y-coordinate of the sphere in each frame were determined by clicking on the centre of the sphere using ImageJ's built-in measurement tool (crosshair). Images were calibrated for length by imaging a ruler at the same location of the falling spheres. The sphere's position data were imported into MATLAB and converted to position versus time. The average and standard deviation of the terminal velocity was calculated for five spheres for each sphere size.

While low Reynolds number flows are characterized by small velocity gradients, their length scales are long, and so the movement through the fluid can be affected by boundaries. This effect in falling ball viscometry is well known and so we used a correction factor to account for the wall proximity [8]:

$$v_{\mathrm{exp}} = \frac{v_{\mathrm{meas}}}{1 - 2.104(d/D) + 2.089(d/D)^3} \tag{12}$$

where v_{meas} is the experimentally measured terminal velocity, d is the diameter of the sphere, D is the diameter of the cylinder, and v_{exp} is the expected velocity of the sphere if it were falling in an unbounded fluid.

The logarithm of the average terminal velocity versus the logarithm of the radius is shown in figure 2 for both the observed and corrected terminal velocities. The Reynolds number for the spheres ranged from 4.1×10^{-3} to 33×10^{-3}, well within the low Reynolds number range assumed for the linear drag model. For the corrected velocity we obtained an exponent of $a = 2.0 \pm 0.1$ (95% confidence), which is the expected quadratic relationship.

3.2. High Reynolds number

To reach high Reynolds numbers, we dropped stainless steel spheres ($r = 0.08$–0.32 cm) into 1000 ml graduated cylinders filled with water. We measured the viscosity of water to be 9.8×10^{-3} g cm^{-1} s^{-1} with a falling ball viscometer and we took the density of water to be 1 g cm^{-3} and the density of stainless steel to be 8.02 g cm^{-3}. We choose the size of the cylinder to be sufficiently tall to allow the spheres to reach terminal velocity. Since the terminal velocity of the spheres in water is much larger than in glycerol, we used a different method to measure the velocity of the sphere. As before, we acquired frames of the sphere falling from the point of release. But for the high Re case, we adjusted the shutter speed of the camera so that during

[3] LabVIEW, National Instruments, Austin, TX.
[4] Wayne Rasmuth, NIH, Bethesda, MD.
[5] MATLAB 7, The Mathworks Inc, Natick, MA.
[6] Sigma-Aldrich, St Louis, MO.

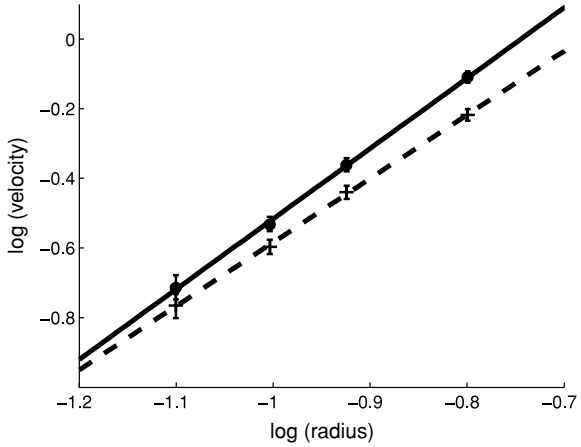

Figure 2. Plot of average terminal velocity versus radius for the aluminium spheres ($n = 5$) in glycerol. Error bars represent standard deviations, but some are smaller than the plot markers. The solid line is the fit to the corrected velocity (•) and the dashed line is the fit to the uncorrected velocity values (+) using (12). From a least-squares linear fit ($\log v_{\text{ter}} = a \log r + b$) to the uncorrected velocity, we obtained $a = 1.8$ and $b = 1.25$ with an R^2 of 1.00, and for the fit to the corrected velocity, $a = 2.0$ and $b = 1.5$, with an R^2 of 1.00.

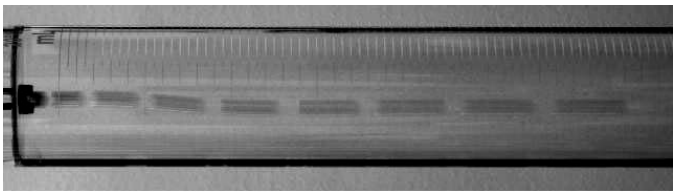

Figure 3. A montage of images of a steel sphere (0.24 cm radius) falling in a graduated cylinder filled with water. The image has been rotated and so the sphere is falling from left to right. Each image was taken at 30 frames per second. The exposure time was 25 ms.

each frame capture, the distance that the sphere moved could be determined by measuring the length of its blurred image (figure 3). The sphere velocity for each frame was calculated by dividing this measured distance by the exposure time.

The logarithm of the average terminal velocity plotted as a function of the logarithm of the radius can be seen in figure 4. The Reynolds number ranged from 920 to 7500. A curve fit to the data produced an exponent of $a = 0.46 \pm 0.07$ (95% confidence), which is close to the predicted one-half power relationship.

At high Reynolds number, the sphere's approach to terminal velocity is slow enough to be measured with our system (figure 3). We chose a sequence of images that showed an initial velocity as close as possible to zero at the time of release and calculated the velocity of the sphere using the same method as above. The approach to terminal velocity for a single sphere shows a reasonable match to the general solution (figure 5).

4. Discussion

The experiment as described effectively demonstrates the velocity dependence of drag at high and low Reynolds number. Students are introduced to a general theoretical framework that

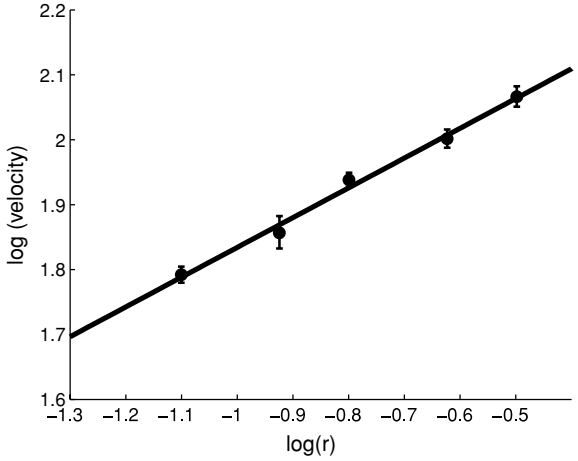

Figure 4. Plot of average terminal velocity versus radius for the stainless steel spheres ($n = 5$) in water. Error bars indicate the standard deviation. From a linear fit ($\log v_{\text{ter}} = a \log r + b$) we obtained $a = 0.46$ and $b = 2.3$ with an R^2 of 0.96.

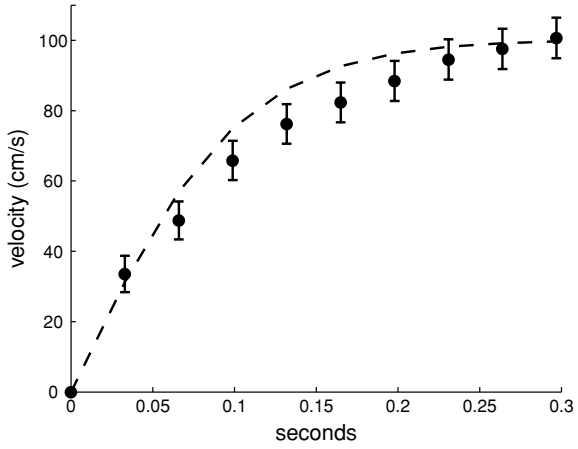

Figure 5. Plot of approach to terminal velocity for a stainless steel sphere ($r = 0.159$ cm) in water. The dashed line is a plot of $v(t) = a \times \tanh((g/a) \times t)$, where g is the acceleration due to gravity, and $a = 100.3$ cm s^{-1} is the measured terminal velocity. Error bars indicate uncertainty due to the measurement resolution of 1 pixel.

can be applied to two limiting conditions and perform experiments using scaling relationships to verify the applicability of the theory in these two cases.

The design of the experiment is simple enough to be assembled by first-year students and compact enough to be performed on the desktop or a small section of lab bench. The semi-automated methods of data collection removed much of the tedium associated with laboratories in this general category, and allowed measurements accurate enough for most students to get excellent agreement between theory and measurement. The computer imaging and measurement techniques used here can be accomplished with a variety of systems at a lower cost than what has been described. For example, inexpensive 'webcams' and image

capture programs are available for both Microsoft Windows-based and Macintosh computers, and the public domain image processing program, ImageJ, is freely available.

The experiment was performed by 35 first-year students, as a first experiment, in a new integrated science course. General feedback from the students was positive. To try and avoid the typical pre-fabricated nature of many introductory laboratories, we had students assemble their experimental setups from supplied parts and run preliminary experiments to optimize their final configuration. The students found the computer video-based imaging and measurement to be intuitive. Execution of the experiment was well within the capability of all the students and most got satisfactory fits to their high and low Reynolds number data. Some students using MATLAB for the first time had difficulty and needed to resort to more familiar tools such as EXCEL or calculators, but none had problems manipulating and fitting the data. The most advanced students were challenged by the derivation of the general solutions to the equation of motions while students with the least preparation could handle the simpler derivations of the terminal velocity and scaling relations.

Acknowledgments

The authors would like to thank the students who took part in the lab and gave us useful feedback, and also Alex DeWolfe who measured the camera shutter speed. Course development was supported by a Center grant from the National Institute of General Medical Sciences (GM 071508) and a generous gift from Richard M Fisher.

References

[1] Purcell E M 1977 *Am. J. Phys.* **45** 3
[2] Tipler P A and Mosca G 2004 *Physics for Scientists and Engineers* (New York: Freeman)
[3] Bisquert J, Ramirez P, Barbero A J and Mafe S 1991 *Eur. J. Phys.* **12** 249
[4] Hart F and Little C 1976 *Am. J. Phys.* **44** 872
[5] Vogel S 1994 *Life in Moving Fluids* (Princeton, NJ: Princeton University Press)
[6] Brown P P and Lawler D F 2003 *J. Environ. Eng.* **129** 222
[7] White E 1974 *Viscous Fluid Flow* (New York: McGraw-Hill)
[8] Lommatzsch T, Megharfi M, Mahe E and Devin E 2001 *Metrologia* **38** 531